Available online at www.sciencedirect.com
ScienceDirect
Acta Materialia 56 (2008) 282–291
Acta MATERIALIA
www.elsevier.com/locate/actamat

Rotational diffusion and grain size dependent shear instability in nanostructured materials

Shailendra P. Joshi, K.T. Ramesh *

Department of Mechanical Engineering, The Johns Hopkins University, 3400 North Charles Street, Baltimore, MD 21218, USA

Received 26 June 2007; received in revised form 13 September 2007; accepted 15 September 2007
Available online 7 November 2007

Abstract

Previous experimental observations on some nanostructured metals have indicated a transition from homogeneous to non-homogeneous plastic deformation with a reduction in grain size [Jia D, Ramesh KT, Ma E. Acta Mater 2003;51:349]. We present a model that predicts the development of shear bands in such materials under quasi-static loading rates. Motivated by microscopic observations, a grain rotation based geometric softening mechanism is implemented as an internal variable within a viscoplastic constitutive setting. The model predicts the occurrence of the shear bands at small grain sizes, whereas at larger grain sizes it predicts homogeneous plastic flow. The model also predicts the phenomenon of shear band broadening with strain, which is experimentally observed, and attributes this to the "rotational diffusion" mechanism along with the restoration of material hardening within the band following the saturation of grain reorientation. Finally, we provide a localization index that can be used to classify nanostructured metals in terms of the susceptibility to this shear band mechanism.

Keywords: Nanostructured metals; Shear banding; Geometric softening; Grain rotation

1. Introduction

The impressive mechanical strengthening in bulk nanostructured (NS) materials is associated with novel microscopic deformation mechanisms, which together determine the overall mechanical response. Detailed overviews of the mechanical behavior of nanocrystalline materials provide insights into the deformation mechanisms that may occur within the grains and at the grain boundaries (GBs) as a function of grain size [1,2]. In the nano-regime of grain sizes, experimental observations [3–6], theoretical models (e.g. [4]), and molecular dynamics simulations (e.g. [7]) have indicated activation of novel deformation mechanisms such as grain rotation, GB sliding and GB migration to accommodate plastic flow. On a macroscopic scale, a characteristic feature observed in the constitutive response of many (but not all) NS materials is the lack of strain hardening beyond small strains. Further, a clear trend has emerged with respect to the strain rate sensitivity (SRS) in the case of pure metals; for body-centered cubic (bcc) structures the SRS decreases as the grain size decreases, whereas the reverse is true for face-centered cubic (fcc) structures [8]. In bcc structures, the lack of strain hardening and SRS results in an increased propensity to inhomogeneous plastic deformations under applied load. Indeed, Carsley et al. [9] reported intense shear banding under quasi-static compression for an Fe–10Cu alloy over a wide range of grain size (45 nm–1.7 μm). Jia et al. [10] systematically studied the strain rate dependence and modes of plastic deformation for consolidated iron over a wide range of compressive strain rates (10^{-4}–10^{+4} s^{-1}) and grain sizes (80 nm–1 μm). They observed that at grain sizes below 300 nm the deformation progressed by shear band nucleation, propagation and broadening with applied load; however, at larger grain sizes the material exhibited homogeneous plastic flow. Similar observations have been made in vanadium and tungsten [11,12]. Through transmis-

* Corresponding author. Tel.: +1 410 516 7735; fax: +1 410 516 7254.
E-mail address: Ramesh@jhu.edu (K.T. Ramesh).

1359-6454/$30.00
doi:10.1016/j.actamat.2007.09.031

sion electron microscopy (TEM) observations (Fig. 1) of nano-Fe, Wei et al. [13] showed that the grains experienced rotation and alignment during deformation to form bands with textures that allow easy slip in certain orientations. Further, they also observed uniform microstructures and the absence of recrystallization in the bands, minimizing the possibility of temperature effects. Based on these characteristics, the authors postulated a geometric softening mechanism involving grain rotation that results in the localization of plastic flow.

Several researchers have investigated shear banding due to textural softening and lattice reorientation in single crystals and coarse-grained polycrystals under different states of loading [14–18]. However, few theoretical investigations of shear banding in bulk NS materials as a function of grain size have been undertaken. The conventional continuum approach cannot predict such size effects because of the absence of a length-scale in the governing equations. To circumvent this problem, strain gradient plasticity theories have been applied to this problem [19–21]. However, these gradient plasticity theories do not explicitly account for grain size. Augmented crystal plasticity models have been employed to investigate the overall behavior of NS materials by invoking an independent constitutive description for grain boundaries [22] or through gradient based constitutive laws for slip system hardening rates [23]. These numerical models are capable of computing widths of localized deformation bands while minimizing the pathological effects of the underlying mesh discretization.

In this article, we present a different approach to model the growth of shear bands in NS and ultrafine-grained (UFG) materials subjected to quasi-static rates of loading. The model considers the development of shearing instabilities through a viscoplastic constitutive law for the material response coupled with micromechanics-based geometric softening driven by grain rotation, motivated by the observations of Jia and co-workers [10,13]. The grain size enters naturally through the grain rotation mechanism. In the following section, we describe the model and set up the governing equations.

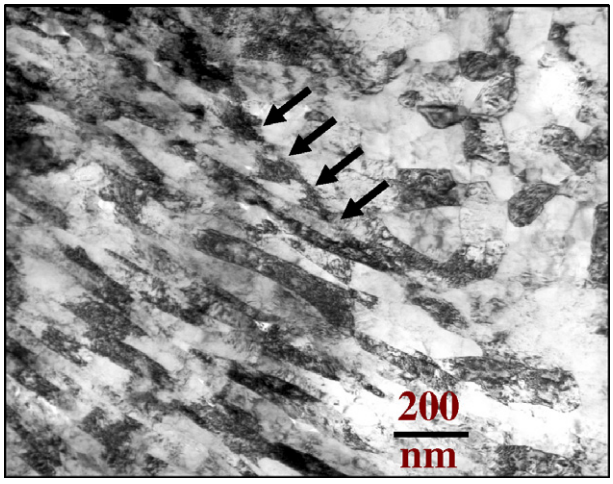

Fig. 1. Bright-field TEM image showing elongated grains inside a shear band that are oriented along the shear band direction and equiaxed grains outside the shear band. Note relatively sharp boundary of the shear band. The average grain size is 110 nm. (Courtesy Dr. Q. Wei.).

2. Model description

A one-dimensional shear problem is considered with an infinitely long slab with finite thickness W (in the X direction), subjected to a constant nominal shear strain rate ($\dot{\gamma}_a$). In the absence of inertial effects the momentum balance equation reduces to an equilibrium equation, $\frac{\partial \tau}{\partial X} = 0$, where τ is the shear stress. We assume that the problem is isothermal. The material is assumed to be elastic/viscoplastic, so that

$$\dot{\tau} = \frac{\partial \tau}{\partial t} = \mu \bar{\dot{\gamma}}_e = \mu(\dot{\gamma}_a - \bar{\dot{\gamma}}_p), \tag{1}$$

where μ is the elastic shear modulus, $\bar{\dot{\gamma}}_e$ is the average elastic strain rate and $\bar{\dot{\gamma}}_p$ is the average plastic strain rate $(= \frac{1}{W}\int_0^W \dot{\gamma}_p \, dX)$, and the total applied strain rate is $\dot{\gamma}_a = \bar{\dot{\gamma}}_e + \bar{\dot{\gamma}}_p$.

A viscoplastic constitutive law is assumed for the evolution of plastic strain,

$$\dot{\gamma}_p = \dot{\gamma}_0 \left\langle \left\{ \frac{\tau}{\tau_0} \frac{1}{(1 - \bar{c}\phi)} \left(1 + \frac{\gamma_p}{\gamma_0}\right)^{-n} \right\}^{1/m} - 1 \right\rangle, \tag{2}$$

where $\langle \cdot \rangle$ is defined as $\langle f \rangle = (f + |f|)/2$, ϕ is an internal variable defined as the number fraction of grains in a given region that have the soft orientation aligned to the shearing direction and γ_p is the plastic strain. The terms $\dot{\gamma}_0, \tau_0, \gamma_0$, n and m in Eq. (2) represent the characteristic strain rate, yield strength (of the polycrystalline material), yield strain (corresponding to τ_0), strain-hardening index and strain-rate sensitivity, respectively. The factor $\bar{c}$ is defined as $\bar{c} = 1 - \frac{\tau_{s0}}{\tau_{h0}}$, where τ_{h0} and τ_{s0} are the yield strengths of the grains in the hard and soft orientations (corresponding to a single crystal).

2.1. Definition of internal variable

Consider a representative volume element (hereafter referred to as a bin or RVE) that contains a large number of grains N_b. Then $\phi(t) = N_s/N_b$, where N_s is the number of grains in the bin that have the soft orientation aligned with the shearing direction, and the evolution of ϕ represents the evolution of rotation of the grains. Thus, as more and more grains rotate into the soft shearing orientation, a softening mechanism develops. We demonstrate that this softening mechanism leads to localization, with a shear band that is essentially the region where $\phi \approx 1$.

We assume that ϕ evolves through contributions from two specific mechanisms, so that

$$\dot{\phi} = \dot{\phi}_1 + \dot{\phi}_2. \tag{3}$$

The first component $\dot{\phi}_1$ in Eq. (4) represents the contribution of overall plasticity (Fig. 2a) to grain rotation, while

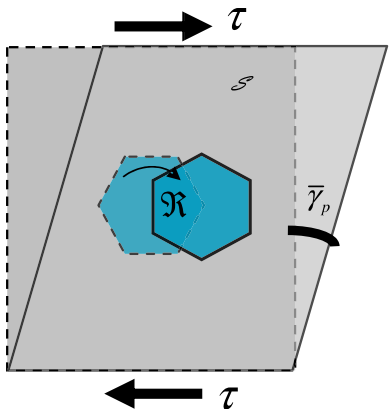

Fig. 2a. Schematic of the rotation of ensemble of nano-grains occupying region $\mathfrak{R}$ embedded in a viscoplastic sea $\mathscr{S}$ subjected to shear. The dotted image shows the undeformed configuration.

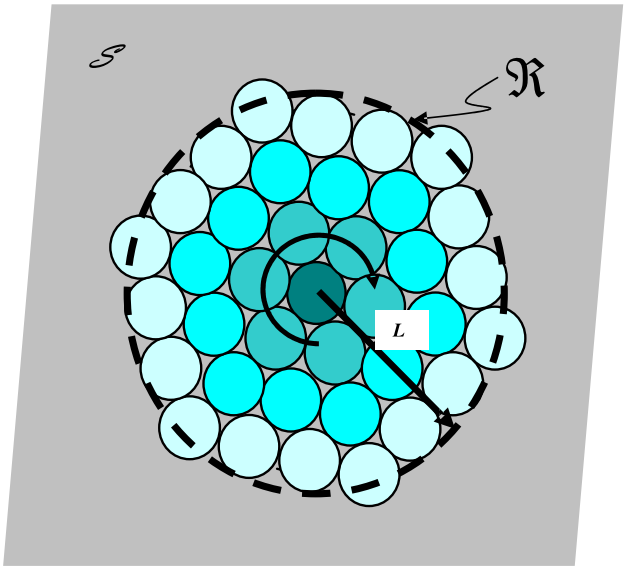

Fig. 2b. Enlarged view of $\mathfrak{R}$ showing intergranular interaction in the region. Rotation of central grain is accommodated by rotation of surrounding grains over length L.

$\dot{\phi}_2$ represents the contribution due to interaction of a grain with nearest neighboring grains (Fig. 2b). ϕ ceases to grow once it reaches unity (since no further reorientation is possible), so that $\dot{\phi} = 0$ when $\phi = 1$.

2.1.1. Contribution of overall plastic deformation

We focus on the contribution to rigid rotation of an ensemble of grains ($\mathfrak{R}$) due to overall plastic deformations in the viscoplastic sea ($\mathscr{S}$) surrounding the ensemble (Fig. 2a). Strain compatibility at the interface of $\mathfrak{R}$ and $\mathscr{S}$ gives a rotation rate that is proportional to the rate of plastic deformation. Thus, the contribution of overall plastic deformation to the evolution of ϕ is given to first-order by

$$\dot{\phi}_1 = \psi(\phi, \bar{d})\dot{\gamma}_p, \tag{4}$$

where $\bar{d}$ is the mean grain size within the ensemble.[1] The function ψ indicates the ease with which the ensemble $\mathfrak{R}$ can rotate rigidly in the sea. An ensemble residing in a region where surrounding grains are soft ($\phi > 0$) will rotate with relative ease as the soft surrounding medium deforms plastically. On the other hand, in a region where the grains are randomly oriented, rotation (in the direction consonant with macroscopic shear) is difficult because the surrounding grains will not deform easily. Further, ensembles with very small $\bar{d}$ will tend to rotate to accommodate the global plastic deformations, while those with large $\bar{d}$ will tend to deform plastically through crystallographic slip. The mean grain size in the ensemble is determined from the grain size distribution, and in this way the grain size distribution may affect $\dot{\phi}_1$. We choose to ignore these variations within the current work, and write $\psi(\phi, \bar{d}) = \psi_0$, where ψ_0 is of order 1–10 (a macro–micro dissipation balance shows that ψ_0 can be approximately 10 for NS materials, given the grain size strengthening).

2.1.2. Contribution of intergranular interaction

Grain rotation may also be caused by the local interactions of a single grain with its neighboring grains of similar size. Grain rotation models based on interfacial contact resistance have been successfully implemented in simulating granular flow [24] including elastoplastic contact [25]. We include this elastoplastic contact mechanism through a hierarchical scheme to model NS polycrystalline metals. Using a three-grain model, we employ the concept of interfacial interaction at the grain level to determine a driving force for rotation; subsequently, an evolution law for grain rotation is prescribed in terms of the driving force.

2.1.2.1. Grain rotation due to interface traction—a three-grain model. As noted by Iwashita and Oda [24] for granular materials, individual grains may be biased to rotate in one direction in the presence of rolling contact resistance. Due to rolling resistance, neighboring grains create interfacial traction that can be expressed using the equations for elastoplastic contact. Utilizing this concept, we consider interaction between three adjacent grains as shown in Fig. 3.

Let the current rotation angles of the three grains a, b and c in Fig. 3D be denoted as θ_a, θ_b and θ_c, respectively. Focusing on the central grain (b) and assuming ($\theta_a > \theta_b > \theta_c$), the interfacial tractions on grain b are specified as $F_{ab} = (k_t\delta_t)_{ab}$ and $F_{bc} = (k_t\delta_t)_{bc}$, where k_t is the effective contact stiffness and the relative tangential displacements are of the form $(\delta_t)_{ab} = \{(\delta_t)_a - (\delta_t)_b + R_a(\theta_a) - R_b(\theta_b)\}$, with R_a and R_b denoting the radii of grains a and b. If we ignore the sliding of grains (i.e. $(\delta_t)_a - (\delta_t)_b = 0$) and assume identical grains of mean diameter d, we get

[1] We note that this dependence on $\dot{\gamma}_p$ can also be obtained by consideration of the plastic spin, along the lines defined by Dafalias and co-workers.

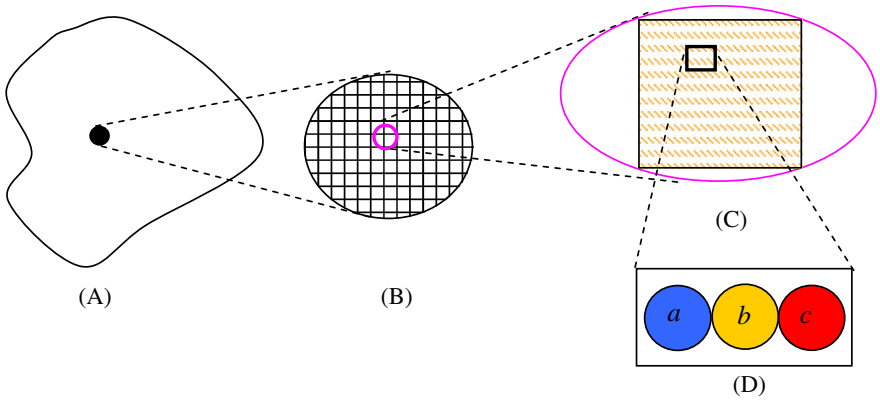

Fig. 3. A hierarchical approach to homogenization of grain rotation due to interface traction. (A) Material continuum, (B) collection of bins in sample space, (C) grains within a RVE. The colored shading represents the average grain orientation in that bin. (D) Interaction at the grain level. Grains with individual orientations are shown in different colors.

$$(\delta_t)_{ab} = \frac{d}{2}(\theta_a - \theta_b) \quad \text{and} \quad (\delta_t)_{bc} = \frac{d}{2}(\theta_b - \theta_c). \tag{5}$$

Using Eq. (5) the net interface traction per unit length $[\Delta F]_b = [F_{ab} - F_{bc}]$ experienced by grain b is $[\Delta F]_b = \frac{k_t d}{2}[\theta_a - 2\theta_b + \theta_c]$ and the net torque is therefore

$$T_b = \frac{d}{2}[\Delta F]_b = \frac{k_t d^2}{4}[\theta_a - 2\theta_b + \theta_c]. \tag{6}$$

The contact stiffness of the grains undergoing elastoplastic deformation in terms of the radius (a) of the contact area is [26] $(k_t)_{ab} = \frac{8a}{C_{ab}}$ with $C_{ab} = \frac{2-\nu_a}{\mu_a} + \frac{2-\nu_b}{\mu_b}$ being the contact compliance between two grains defined by the shear modulus (μ) and Poisson's ratio (ν) for each grain.[2] The radius (a) of the contact area depends on the applied stress and determines whether the contact is elastic, elastoplastic or fully plastic [26]. In general, the contact area will evolve as grains rotate [27,28]; here, we assume a fully plastic contact for this polycrystalline material and set the radius of the contact equal to the grain radius ($a = d/2$). The driving force for grain rotation is then given by Eq. (6). We postulate a kinetic relation between the evolution of grain rotation and the driving force; let the rate of rotation be given by

$$\dot{\theta}_b = (m_r T)_b, \tag{7}$$

where m_r is the mobility representing the resistance provided by the surrounding grains to the rotation of grain b. Eq. (7) is similar to those adopted in describing grain rotation coalescence [29,30]. In the latter work the driving force is due to anisotropic GB energies and the plastic deformation is accommodated by GB and lattice diffusion mechanisms, which are believed to be dominant at very small grain sizes ($d < 10$ nm) and at elevated temperatures. Van Swygenhoven and Caro [31] hypothesized a GB-dominated viscoplastic model to describe nano-grain rotation ($d \approx 3$–5 nm) at very low temperatures where diffusion mechanisms are not active. Similarly, in defining the mobility, we account for the viscoplastic resistance offered by the region surrounding the rotating grain.

The rotation of any single grain must be accommodated by the surrounding grains (and the grain boundaries), and there is a finite length (L) over which this accommodation occurs (Fig. 2b). That is, grains sufficiently far away from the rotating grain are unaffected by the rotation. This length scale for rotational accommodation will be smaller for elastoplastic grains[3] (as in polycrystalline metals) than for purely elastic grains (a limiting example of which would be sand). The mobility due to the viscoplastic resistance is

$$(m_r)_b = \frac{1}{L^3}\left(\frac{1}{\eta_e}\right), \tag{8}$$

where η_e is the effective viscosity ($\frac{1}{\eta_e} = \frac{1}{\eta_p} + \frac{1}{\eta_{gb}}$) of the accommodating region and has contributions from dislocation plasticity (η_p) and GB mechanisms (η_{gb}). The effective viscosity corresponding to GB sliding is $\eta_{gb} = \frac{kTd^3}{64\delta\Omega D_{gb}}$, where k is the Boltzmann constant, T is the temperature, δ is the GB thickness, Ω is the atomic volume and D_{gb} is the GB diffusion coefficient [2]. The contribution to the effective viscosity (η_p) from dislocation plasticity could be represented by the viscoplastic resistance provided by the grains, a phenomenological lower bound for which is $\tau_{s0}/\dot{\gamma}_0$ (one other estimate would be $\tau_0/\dot{\gamma}_0$). The form of η_e adopted in the model could also be estimated through molecular dynamics simulations (e.g. [31]).

In Eq. (8), one would expect L to be of the order jd, where j is the number of other grains involved. This length scale ($L = jd$) is a natural length scale for a bin. Since very large grains will deform by slip rather than rotate, we assume that L is a fixed length scale for a given material and the number of grains involved in accommodating the rotation are $j = L/d$. In a nano-grained material, more than one grain ($j > 1$) is accommodated over L. For larger grain

[2] Note that C_{ab} could be modified to include GB properties, but we choose to ignore these at this point.

[3] Note that the plasticity allows for deformation at triple points and corners and also avoids the development of dilatation.

sizes, when $j < 1$, we assume that this grain rotation mechanism is not possible and slip is the only mode of deformation. A precise quantitative measure of L remains to be established. For example, L can be viewed in a manner analogous to the microstructural length scales derived in strain gradient plasticity theories [32].

2.1.2.2. Homogenized representation of grain rotation. We now derive an expression for $\dot{\phi}_2$ by homogenizing the evolution of θ over the RVE (Fig. 3C). The average grain orientation over the RVE is, $\bar{\theta} = \frac{1}{N_b}\sum_{k=1}^{N_b}|\theta_k|$. We count the number of favorably oriented grains by performing a weighted averaging with a penalty function ζ_k in the form of a delta function, $\zeta_k = \delta(|\theta_k| - \theta_s)$ where θ_s is the favorable orientation (aligned with the band orientation). In terms of the internal variable, as $\bar{\theta} \to \theta_s$, $\phi \to 1$. Thus, for the RVE we have $\phi_2 = \frac{1}{N_b}\sum_{k=1}^{N_b}\zeta_k|\theta_k|$. The average rate of change of ϕ_2 for the RVE is (using the kinetic relation):

$$\dot{\phi}_2 = \frac{1}{N_b}\sum_{k=1}^{N_b}\zeta_k\dot{\theta}_k = \frac{1}{N_b}\sum_{k=1}^{N_b}\zeta_k(m_r T)_k. \tag{9}$$

Using Eq. (6), we thus obtain

$$\begin{aligned}\dot{\phi}_2 &= m_r\frac{k_t d^2}{4N_b}\sum\zeta_k(\theta_a - 2\theta_b + \theta_c)\\ &= \frac{k_t d}{4j\eta_e}\left[\frac{1}{j^2 d^2 N_b}\sum\zeta_k(\theta_a - 2\theta_b + \theta_c)\right].\end{aligned} \tag{10}$$

Using Eq. (10), we identify the terms in the square brackets as approximating the second derivative $\frac{\partial^2\phi}{\partial X^2}$ in the continuum limit, so that:

$$\dot{\phi}_2 = \left(\frac{k_t d}{4j\eta_e}\right)\frac{\partial^2\phi}{\partial X^2} = D_r\frac{\partial^2\phi}{\partial X^2}, \tag{11}$$

where $D_r = \frac{1}{j\eta_e}\left(\frac{\mu d^2}{2-\nu}\right)$. Eq. (11) may be viewed as a rotational diffusion mechanism that tends to diffuse variations in ϕ through intergranular interactions. Eq. (3) together with Eqs. (4) and (11) provides the net evolution of the internal variable as

$$\dot{\phi} = \psi\dot{\gamma}_p + D_r\frac{\partial^2\phi}{\partial X^2}. \tag{12}$$

With our definition of η_e a transition from dislocation-dominated mobility to GB-dominated mobility will occur at $d_{tr} = \left(\frac{64\delta\Omega D_{gb}\tau_{s0}}{kT\dot{\gamma}_0}\right)^{1/3}$ (≈8.6 nm in the case of iron, for example), so that η_{gb} might be dominant for smaller grain sizes. Note that below the transition grain size $D_r \propto d^{-1}$. However, this inverse dependence is compensated by j (due to its d^{-1} dependence for fixed L), which eliminates grain size effect in the rotational diffusion mechanism. This implies that below d_{tr} band broadening may be small, at a rate that is constant and independent of the grain size. In what follows, we do not consider the contribution from GB's to the effective viscosity and retain only the contribution from the intragranular viscosity (η_p).

The governing equations for the problem are now summarized below:

$$\frac{\partial\tau}{\partial X} = 0 \tag{13a}$$

$$\frac{\partial\tau}{\partial t} = \mu(\dot{\gamma}_a - \bar{\dot{\gamma}}_p) \tag{13b}$$

$$\dot{\gamma}_p = \dot{\gamma}_0\left\langle\left\{\frac{\tau}{\tau_0}\frac{1}{(1-\bar{c}\phi)}\left(1+\frac{\gamma_p}{\gamma_0}\right)^{-n}\right\}^{1/m} - 1\right\rangle \tag{13c}$$

$$\dot{\phi} = \psi\dot{\gamma}_p + D_r\frac{\partial^2\phi}{\partial X^2}. \tag{13d}$$

We integrate these equations numerically using the procedures described in the following section.

3. Model implementation

An infinitely long slab is subjected to a quasi-static nominal shear strain rate. The initial conditions are, $\tau(X, 0) = 0$, $\phi(X, 0) = \phi_i(X)$, $\gamma(X, 0) = 0$, $\dot{\gamma}(X, 0) = \dot{\gamma}_a$. Eqs. (13a)–(13d) are solved numerically using the finite-difference method and integrated using the Euler forward difference scheme.[4] We begin by considering a model case with default values for the various parameters listed in Table 1 (corresponding to NS-Fe). We assume an initial defect distribution ϕ_i in the form of a Gauss function, $\phi_i(X) = \phi_\infty + \phi_0\exp[-A(X/W - 0.5)^2]$, where ϕ_0 and ϕ_∞ are respectively the maximum and the far field initial values of ϕ; A is a dimensionless parameter akin to wavenumber. We set $\phi_\infty = 0$.

As an illustrative case, we consider a slab ($W = 300$ μm) of polycrystalline iron (Table 1, [10,33]) subjected to a nominal shear strain rate ($\dot{\gamma}_a$) of $1\times10^{-3}\,s^{-1}$. The slab is discretized into 20,000 segments with 20,001 nodes ($\Delta X = 15$ nm). Given the heavy plastic work during severe plastic deformation processes, the parameter $\bar{c}$ is obtained at large strains (~1) from the results of Spitzig and Keh [34] on iron single crystals.

For a material with this initial distribution in ϕ, Fig. 4 shows the evolution of ϕ as a function of nominal strain near the band. ϕ increases rapidly at the center of the initially perturbed region at $\gamma \sim 0.02$, and stops evolving ($\dot{\phi} = 0$) once it reaches the maximum value ($\phi = 1$) in the center. Physically, this represents a stage where following the localization and the stress-drop the grain reorientation process saturates and no further reorientation occurs in that region. At the onset of severe localization, the plastic shear strain rate (not shown) is very high ($\sim 10^3\dot{\gamma}_a$) in the band center while it drops in the rest of the region. With increasing nominal strain, $\dot{\gamma}_p$ drops in the band center (in this strain-hardening case) because ϕ is constant but the plastic strain continues to grow. Following a fully developed band (characterized by a finite thickness over which $\phi = 1$), $\dot{\gamma}_p$ at the edges of the band remains high where ϕ has not saturated. Subsequent band growth is driven by

[4] The stability of solution is ensured by maintaining a time step smaller than that required by the Courant condition for a prescribed spatial discretization.

Table 1
Default material parameters for simulations, corresponding to polycrystalline Fe

Parameter	d, nm	μ, GPa	ν	$\dot{\gamma}_0$, s^{-1}	τ_0, MPa	n	m	τ_{s0}[a], MPa	$\bar{c}$	ψ	A	ϕ_0, ϕ_∞	L, μm
Value	300	76	0.3	5×10^{-4}	900	0.01	0.005	96	0.07	10	5×10^{4}	0.005,0	1.0

[a] Ref. [34].

rotational diffusion and strain hardening. The plastic strain (γ_p) also increases rapidly once localization begins. At later stages ($\gamma > 0.05$), γ_p slows in the band center while simultaneously spreading around the central region. In the band center the saturation condition for ϕ implies that the material response is determined by the strain-hardening parameter (Eq. (2)).

In Fig. 5, the overall stress–strain response for a defect-free material is presented (curve A) and compared with the response obtained from a sample with the perturbation (curve B, solid line). With the perturbation, the sample exhibits a brief period of strain hardening following yield. The strain hardening is followed by a rapid drop in the stress corresponding to severe localization, with the magnitude of the drop determined by the material hardening and the anisotropy parameters. The nominal strain corresponding to the stress collapse is termed the critical strain (γ_{cr}), hereafter. Following the stress drop, a softening response is observed. Such a macroscopic softening response of a strain-hardening material indicates the dominance of geometric softening over material hardening [18]. Although not apparent on curve B (solid line, Fig. 5), the softening regime exhibits serrated behavior in the presence of strain hardening (seen at a higher magnification on the stress–strain curve) due to the competition between the hardening and softening variables. With increasing strain, the grain reorientation saturates ($\phi = 1$) in the localized region. We define a fully developed shear band as a region where ϕ reaches the maximum value and use this definition to also determine the thickness of the shear band. After localization, the material hardening plus the rotational diffusion (Eq. (11)) control the broadening of the shear band. The development of the thickness of the shear band is shown (Fig. 5, curve B') as a function of overall strain.

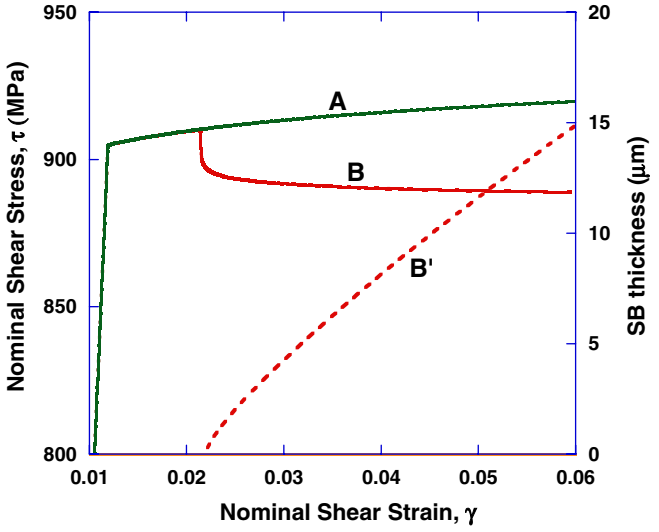

Fig. 5. Overall stress–strain response for a defect-free sample (curve A) and a sample with an initial defect in ϕ (curve B). Curve B′ indicates the development of the shear band thickness corresponding to curve B.

3.1. Effects of ψ and D_r

The governing equations can be rewritten in terms of scaled quantities $\hat{x} = X/L$ and $\hat{t} = \dot{\gamma}_0 t$: $\frac{\partial \tau}{\partial \hat{x}} = 0$; $\frac{\partial \tau}{\partial t} = \mu(\frac{\dot{\gamma}_a}{\dot{\gamma}_0} - \hat{\dot{\gamma}}_p)$; $\hat{\dot{\gamma}}_p = \dot{\gamma}_0 \frac{\partial \gamma_p}{\partial t}$; $\frac{\partial \phi}{\partial t} = \psi \frac{\partial \gamma_p}{\partial t} + (\frac{D_r}{\dot{\gamma}_0 L^2}) \frac{\partial^2 \phi}{\partial \hat{x}^2}$.

The relative importance of the driving and diffusion terms can be understood through the dimensionless susceptibility ratio $\chi = \frac{\psi \dot{\gamma}_0 L^2}{D_r}$ which exemplifies the importance of ψ/D_r for a given L and $\dot{\gamma}_0$. Large values of χ indicate greater susceptibility to localization. Noting that D_r depends on the effective viscosity, a general expression for the susceptibility ratio is $\chi = \alpha(L/d)^3$, where $\alpha = \frac{(2-\nu)\psi\eta}{\mu}$. The strong effect of grain size is evident in χ,

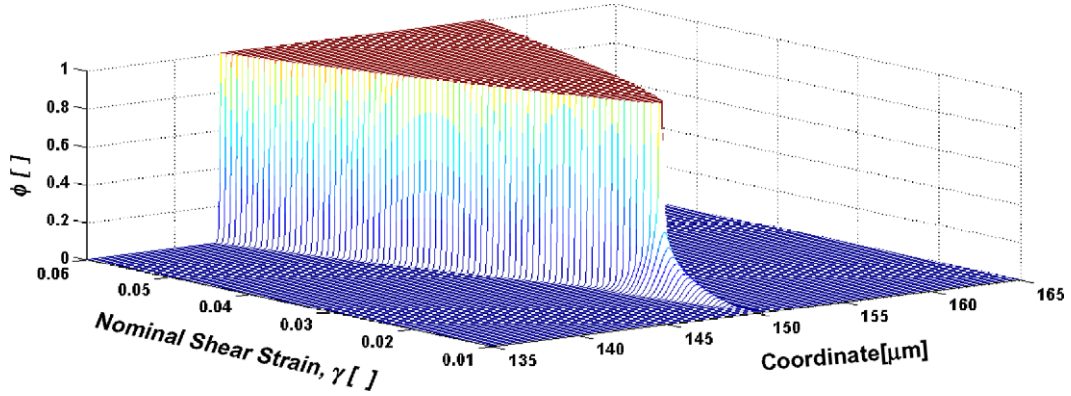

Fig. 4. Evolution of ϕ around the band center.

Table 2
Orientation localization index (α) for several NS metals with a fixed grain size (100 nm)

Material	Crystal structure	μ (GPa)	τ_0 (GPa)	ν	α	Shear band observed? [Ref.]
Tungsten	bcc	161	1.80	0.28	0.19	Yes [12]
Tantalum	bcc	69	0.45	0.34	0.11	No [40]
Iron	bcc	70	1.30	0.29	0.32	Yes [1]
Copper	fcc	48	0.22	0.34	0.075	No [41]
Aluminum	fcc	26	0.21	0.35	0.13	No [35]

indicating that nanostructured materials are susceptible to instabilities. Consider, for example, a comparison of NS metals using $\eta = \tau_0/\dot{\gamma}_0$ so that their current strengths are used, thus accounting for processing effects. The ratio χ then suggests that materials with high overall strength and low stiffness are more likely to localize. We compare different NS metals of identical average grain size in terms of the "orientation localization index" α in Table 2, which indicates that iron (amongst the three bcc materials) and aluminum (amongst the two fcc materials) possess a higher propensity toward the onset of localization. Table 2 also shows that the fcc metals generally are less susceptible than bcc metals to such localization. We note, further, that the strength anisotropy ($\bar{c}$) and strain rate sensitivity will play vital roles in the localization and the NS fcc metals are generally more rate-sensitive than NS bcc metals [8].

3.2. Effect of grain size

The grain size explicitly appears in two quantities in the governing equations: the polycrystalline yield strength (τ_0) in Eq. (2) and the rotational diffusion coefficient D_r in Eq. (11). Let us consider three grain sizes (100 nm, 300 nm and 1 μm), with n and m (0.01 and 0.005, respectively) constant for all the grain sizes under consideration. For illustration purposes, we classify the 100 and 300 nm grain sizes as being in the NS regime, whereas the 1 μm grain size is classified as a coarse-grained material. Using the Hall–Petch relation for Mises yield in iron $\sigma_y = \kappa d^{-1/2}$ ($\kappa = 0.69$ MPa m$^{1/2}$), the shear strengths ($\tau_0 = \sigma_y/\sqrt{3}$) are 1300 (100 nm), 900 (300 nm) and 290 MPa (1 μm).

Fig. 6 shows the band thickness evolution for different grain sizes. Whether a shear band will develop is strongly grain size dependent. If a shear band does develop, the band thickness is larger for larger grain sizes (at equivalent nominal strains), because the rotational diffusion term depends on the grain size. Another length scale that can be determined from the simulations is the transition width of the ϕ profile, indicating the sharpness of the shear band boundary. For fixed ψ, the transition width scales as $\sqrt{D_r}$ and is therefore proportional to grain size (since $D_r \propto d^2$). The simulations show that, for the grain sizes that exhibit shear banding, the transition widths of the ϕ profiles are proportional to grain size. These predictions are qualitatively comparable with the experimental observations of Jia et al. [10] in terms of both band thickness and transition width.

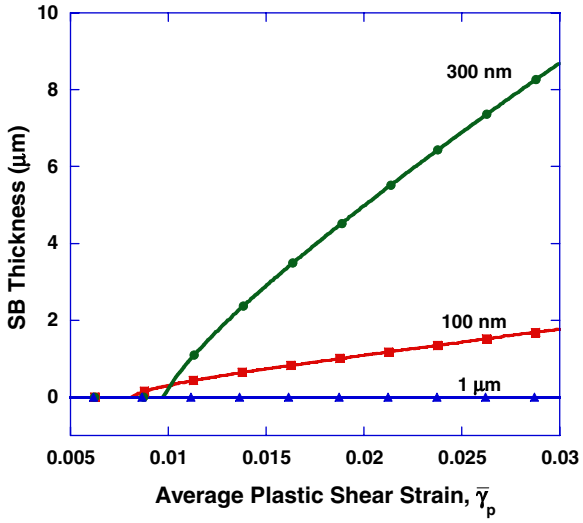

Fig. 6. Evolution of shear band thickness for different grain sizes. The material hardening parameters are held constant for all the grain sizes. The applied strain rate is 1×10^{-3} s^{-1}.

3.3. Comparison with experiments

We consider two quantitative comparisons between the model and specific experiments: (1) bcc-Fe of Jia et al. [10] and (2) fcc-Al of Sun et al. [35]. Note that such comparisons are difficult due to uncertainties in the fine structures and defect densities in real NS materials. Further, both experiments under consideration involved uniaxial loading, whereas the current model is developed for the case of simple shear and considers only a single shear band.[5] However, we seek to distinguish between the two material behaviors using the physics of the model.

3.3.1. NS/UFG iron

Experiments [10,11] show that shear bands occur immediately following yield. Using the material parameters defined earlier (Table 1), this early localization is easily generated if we use a step perturbation ϕ_i that has a maximum value $\phi_0 = 0.3$ and a width of 1 μm. The length scale ($L = 1$ μm) is assumed to be constant for all grain sizes,

[5] Under uniaxial loading conditions one observes the nucleation and growth of multiple shear bands. The gross development of instability of a specimen will in general depend on the defect distributions and specimen geometry. The grain orientation density and distribution may vary from sample to sample, and the real perturbations will play a crucial role in the localization problem.

which in conjunction with the material-hardening parameters determines the broadening rate of the band and the transition width.

In the previous section investigating the grain size effect, the material-hardening parameters were held constant for all the grain sizes. In real bcc structures the hardening parameters may be modified by the grain size due to the variety of processing routes used for generating bulk NS materials. Consolidated Fe [10] exhibits low but finite strain hardening ($n \approx 0.01$–0.04) in the NS regime whereas

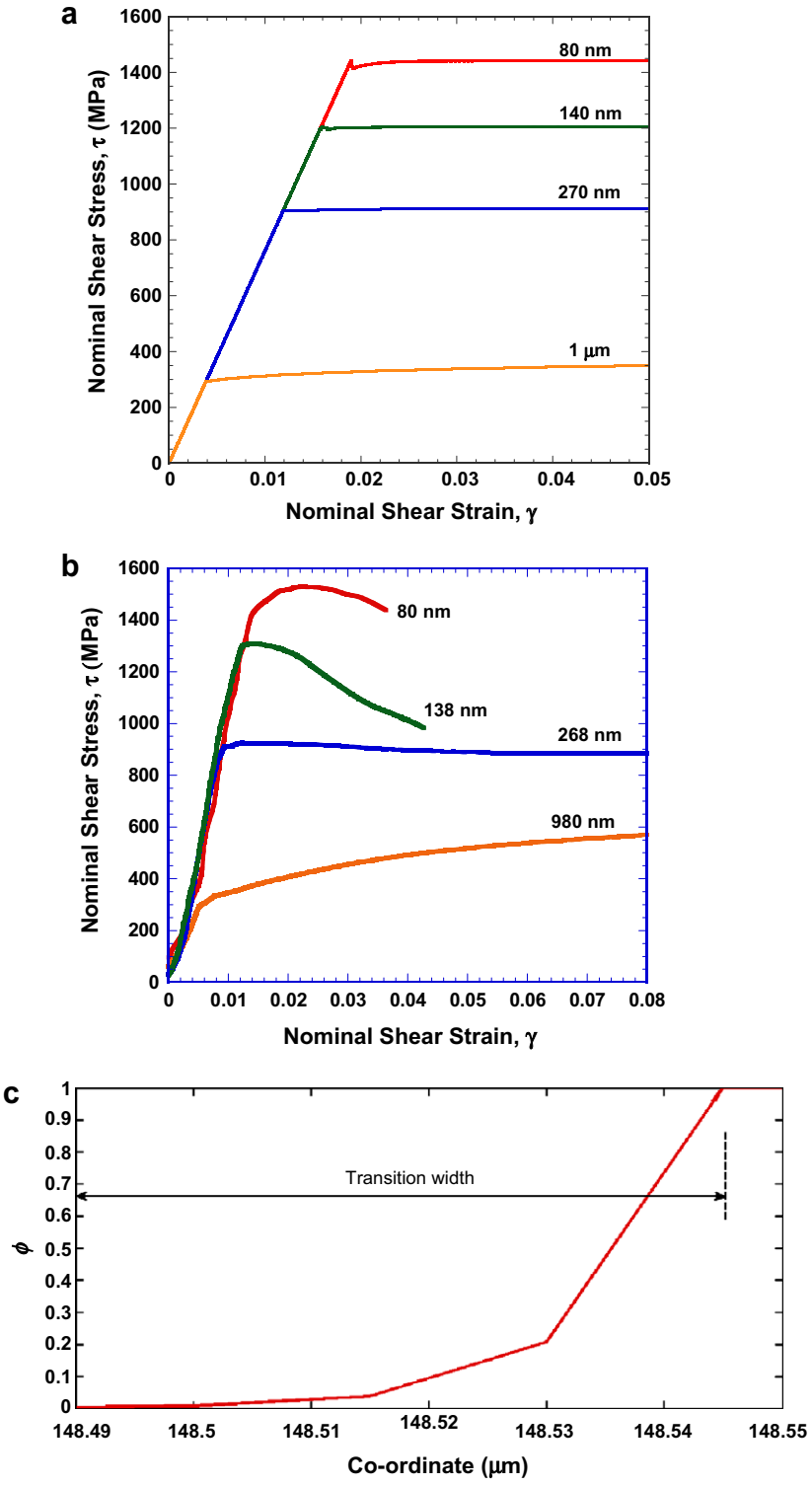

Fig. 7. (a) Effect of grain size on the stress–strain response. Note transition from softening at nano-grain sizes to strain hardening at larger grain size. (b) Experimental stress–strain response [36]. (c) Predicted transition width for 80 nm grain size.

at larger grain sizes n is high ($\approx$0.26) [33]. We assume that strain hardening increases with grain size in NS-Fe using linear interpolation between 80 nm ($n = 0.01$) and 5 μm ($n = 0.26$). We also use linear interpolation for the rate sensitivity [8] (with $m = 0.005$ for $d = 80$ nm and $m = 0.05$ for $d \geqslant 5$ μm).

Using these assumptions, a comparison with the experiments of Jia et al. [10] follows. The stress–strain responses for different grain sizes are obtained for a constant applied strain rate of $5 \times 10^{-4}\,s^{-1}$ (Fig. 7a). For the NS grain sizes the plastic flow shows overall softening, which includes localization (although imperceptible in these macroscopic curves). In contrast, the stress–strain response for the 1 μm grain size exhibits strain hardening, indicating prevalence of the internal material hardening over geometric softening. These results are comparable to the shear stress–shear strain curves obtained from Jia's experiments [36] (Fig. 7b).[6] In the NS regime, the model predicts also that bands occur immediately following yield. The subsequent band growth rates are determined by the material hardening and the rotational diffusion parameters. For the 80 nm case, the model predicts a band thickness of 2.4 μm at a plastic shear strain of about 0.023, which is similar to that reported by Jia et al. [10]. Fig. 7c shows the predicted transition width for the 80 nm case of about 55–60 nm (at nominal strain of 0.05), which is of the order of a grain size (similar observations were made by Wei et al. [13] on 110 nm Fe; see also Fig. 1).

3.3.2. UFG aluminum

Using the same perturbation parameters as in the bcc-Fe case, we compare our model predictions with the experimental observations of Sun et al. [35] on equal channel angular extruded commercially pure aluminum (ECAE-CP-Al). The material hardening parameters are $n = 0.01$ (a low value resulting from saturation of dislocation density due to severe plastic deformation) and $m = 0.044$ [37] for 350, 470 and 590 nm grain sizes and $\bar{c} = 0.15$ [38]. Unlike in the case of the iron, the model does not predict shear banding for these three grain sizes in CP-Al. The quasi-static compression experiments [35] also showed no shear bands for the 350 and 470 nm cases, although apparently anomalous shear bands were observed for the 590 nm case. Our model does not predict shear band development in such rate-sensitive materials as NS and UFG-fcc metals, and in general, shear bands have not been reported in NS or UFG pure fcc metals, although very "diffuse" bands have sometimes been observed in tension. The authors have addressed the rate sensitivity effects in a recent paper focusing on the application of the shear band model to different crystal structures [39].

[6] Note that the experimental softening response in Fig. 10 b is probably caused by the occurrence of multiple shear bands under uniaxial loading conditions.

4. Conclusion

A shear band model has been developed for NS and UFG metals subjected to quasi-static rates of loading. Motivated by microscopic observations, the model incorporates geometric softening in a continuum mechanics framework to predict shear instability in the absence of adiabatic or inertial effects. The geometric softening is controlled by an evolution law for an internal variable that represents grain reorientation. The evolution law invokes a grain rotation mechanism by accounting for two specific contributions: the local rotation driven by gross viscoplastic deformations and a rotational diffusion term arising from intergranular interactions. Analogous to experimental observations, the model predicts inhomogeneous plastic flow through shear banding at small grain sizes, whereas at larger grain sizes it predicts homogeneous plastic flow. The model also captures the phenomenon of shear band broadening that has been reported experimentally and attributes this to rotational diffusion and the restoration of material hardening within the band following the saturation of grain reorientation. The rotational diffusion assists band broadening even in the absence of strain hardening. Our future work will focus on incorporating this model in to a three-dimensional framework and investigating multiple shear band interactions under general loading conditions.

Acknowledgements

Discussions with Prof. Q. M. Wei, Prof. K.Y. Volokh and Dr. C. Eberl are gratefully acknowledged. We thank Prof. Q.M. Wei for the TEM image in Fig. 1. This work was performed under the auspices of the Center for Advanced Metallic and Ceramic Systems (CAMCS) at the Johns Hopkins University, supported by the Army Research Laboratory under the ARMAC-RTP Cooperative Agreement Nos. DAAD19-01-2-0003 and W911NF-06-2-0006.

References

[1] Kumar KS, Van Swygenhoven H, Suresh S. Acta Mater 2003;51:5734.
[2] Meyers MA, Mishra A, Benson DJ. Prog Mat Sci 2006;51:427.
[3] Murayama M, Howe JM, Hidaka H, Takaki S. Science 2002;295:2433.
[4] Cahn JW, Taylor JE. Acta Mater 2004;52:4887.
[5] Gutkin MY, Ovid'ko IA. Appl Phys Lett 2005;87:1.
[6] Yang W, Wang H. J Mech Phys Solids 2004:52.
[7] Haslam AJ, Moldovan D, Yamakov V, Wolf D, Phillipot SR, Gleiter H. Acta Mater 2003;51:2077.
[8] Wei Q, Cheng S, Ramesh KT, Ma E. Mat Sci Eng A 2004;381:71.
[9] Carsley JE, Fisher A, Milligan WW, Aifantis EC. Metall Mat Trans A 1998;29:2261.
[10] Jia D, Ramesh KT, Ma E. Acta Mater 2003;51:3495.
[11] Wei Q, Jiao T, Ramesh KT, Ma E. Scripta Mater 2004;50:359.
[12] Wei Q, Zhang HT, Schuster BE, Ramesh KT, Valiev RZ, Kecskes LJ, et al. Acta Mater 2006;54:4079.
[13] Wei Q, Jia D, Ramesh KT. Appl Phys Lett 2002;81:1240.
[14] Asaro RJ, Needleman A. Acta Mater 1985;33:923.
[15] Dillamore IL. Met Sci 1979;13:73.

[16] Harren SV, Deve HE, Asaro RJ. Acta Metall 1988;36:2435.
[17] Tomita Y. Appl Mech Rev 1994;47:171.
[18] Yang S, Bacroix B. Int J Plasticity 1996;12:1257.
[19] Carsley JE, Milligan WW, Zhu XH, Aifantis EC. Scripta Mater 1997;36:727.
[20] Shi MX, Huang Y, Hwang KC. Int J Mech Sci 2000;42:2115.
[21] Zhu XH, Carsley JE, Milligan WW, Aifantis EC. Scripta Mater 1997;36:721.
[22] Fu H, Benson DJ, Meyers MA. Acta Mater 2004;52:4413.
[23] Kuroda M, Tvergaard V. J Mech Phys Solids 2006;54:1789.
[24] Iwashita K, Oda M. J Eng Mech ASCE 1998;124:285.
[25] Hu N, Molinari JF. J Mech Phys Solids 2004;52:499.
[26] Stronge WJ. Impact mechanics. Cambridge: Cambridge University Press; 2000.
[27] Conrad H, Narayan J. Scripta Mater 2000;42:1025.
[28] Van Swygenhoven H, Derlet PM. Phys Rev B 2001;64:1.
[29] Harris KE, Singh VV, King AH. Acta Mater 1998;46:2623.
[30] Moldovan D, Wolf D, Phillipot SR. Acta Mater 2001;49:3521.
[31] Van Swygenhoven H, Caro A. Appl Phys Lett 1997;71:1652.
[32] Gao H, Huang Y, Nix WD, Hutchinson JW. J Mech Phys Solids 1999;47:1239.
[33] Malow TR, Koch CC, Miraglia PQ, Murty KL. Mat Sci Eng A 1998;252:36.
[34] Spitzig WA, Keh AS. Acta Metall 1970;18:611.
[35] Sun PL, Cerreta EK, Gray GT, Bingert JF. Metall Mat Trans A 2006;37A:2983.
[36] Jia D. PhD Thesis, Johns Hopkins University; 2001. p. 188.
[37] Hayes RW, Witkin D, Zhou F, Lavernia EJ. Acta Mater 2004;52:4259.
[38] Hosford WF. Mechanics of crystals and textured polycrystals. Oxford: Oxford University Press; 1993.
[39] Joshi SP, Ramesh KT. Mat Sci Eng A, accepted for publication.
[40] Wei Q, Jiao T, Mathaudhu SN, Ma E, Hartwig KT, Ramesh KT. Mat Sci Eng A 2006;358:266.
[41] Cheng S, Ma E, Wang YM, Kecskes LJ, Youssef KM, Koch CC, et al. Acta Mater 2005;53:1521.